Constructing Crown Ether-Based Supramolecular Adhesives with Ambient-Temperature Applicable and Durable Adhesion

Hao Ju, [a] *Zhaoliang Yin,* [a] *Zoriana Demchuk,** [b], *Vera Bocharova,* [b] *Catalin Gainaru,* [b] *Jeffrey A. Laub,* [c] *Konstantinos Vogiatzis,* [c] *Rigoberto Advincula,* [d] *Jiayao Chen,** [a] *and Peng-Fei Cao** [a]

* Corresponding author: Dr. Demchuk (demchukz@ornl.gov), Dr. Chen (jiayao.chen@buct.edu.cn) and Dr. Cao (caopf@buct.edu.cn)

[a] State Key Laboratory of Organic-Inorganic Composites, School of Materials Science and Engineering, Beijing University of Chemical Technology, Beijing 100029, China
[b] Chemical Sciences Division, Oak Ridge National Laboratory, Oak Ridge, TN 37830, USA
[c] Department of Chemistry, University of Tennessee, Knoxville, TN 37996, USA
[d] Center for Nanophase Materials Sciences, Oak Ridge National Laboratory, Oak Ridge, TN, 37830, USA

Abstract

Supramolecular adhesives have been attracting considerable attention owing to their dynamic and reversible bonding, while the complex curing conditions and poor performance under extreme conditions severely restricts their applicability. Herein, we present a series of tetra-crown ether-terminated polyethylene glycol (TCE-PEG) adhesives in which plenty of supramolecular interactions, including Van der Waals, hydrogen bonding, π-π staking, metal coordination, and electrostatic ones, provide strong adhesion on multiple types of substrates. Highly relevant for practical applications, ultra-strong adhesivity of TCE-PEG can be achieved without requiring additional ultraviolet radiation, heat, or chemical treatment at ambient temperature. It also exhibits durable adhesive behavior, excellent underwater stability, and low temperature tolerance. Especially, by incorporating ionic polymer fragments of polyethyleneimine hydrochloride, additional hydrogen bonding between secondary amines and crown ether rings can be induced to enhance the lap-shear strength to 7.21 MPa due to the formation of supramolecular cross-linked network. This work pioneers a rather unique supramolecular approach for easily formed, ultra-strong crown-ether-based adhesives bearing great potential for applications in critical environments of limited heat source and unallowed solvent usage.

Keywords: supramolecular chemistry; adhesives; crown ether; noncovalent interactions

1. Introduction

Versatile adhesives are expected not only to achieve strong and tough adhesion to/between desired substrates, but also to preserve their functionality under extreme environmental conditions. The rapid development of supramolecular chemistry and its applications is regarded as the key for overcoming the limitations of traditional polymer adhesives under harsh utilization conditions. To this end, supramolecular adhesives, particularly those with supramolecular polymer networks, have been extensively reported over the past decades due to their desirable functionalities and excellent adhesive performance caused by plentiful dynamic cross-links.[1] Noncovalent interactions including hydrogen bonding,[2] ionic aggregation,[1e, 3] hydrophobic effect,[4] metal-ligand complexation,[5] π-π stacking, Van der Waals[6] and host-guest association,[7] endow the supramolecular adhesion with the assistance of functional groups such as 2-amino-4-hydroxy-6-methylpyrimidine,[1c, 8] cyclodextrin,[9] carboxyl[10] and catechol[11] in macromolecules. By these means, a plethora of unique properties including high strength,[12] self-healing,[13] stimulus response,[14] temperature tolerance,[14b, 15] and water/solvent resistance[1d, 16] has been achieved, rendering supramolecular adhesives as promising candidates in emerging fields such as aerospace, biological science,[6a, 17] soft robotics,[18] and artificial coating applications.[13a, 19]

Crown ethers (CEs), the first generation of macrocyclic hosts in supramolecular chemistry,[20] have been attracting tremendous attentions for complexing a wide range of inorganic and organic cations as well as neutral guest species, owing to their cyclic cavities and electron donating properties.[21] Several studies have employed CEs as side

chains of the building units to fabricate CE-based adhesives[1b, 22] due to the synthesis simplicity and the unique coordination propensity toward the alkali ions that affords high directionality and good selectivity. At present, the synthetic methods of CE-based supramolecular adhesives can be classified into two distinct types: (1) the self-assembly of small molecules or low-molecular-weight monomers (LMWMs),[22a-d] and (2) the noncovalent cross-linking of macromolecules.[1b] The representative instances of LMWMs were reported by Dong and co-workers,[22] who developed a collection of novel CE-based supramolecular adhesives which can maintain excellent adhesive performance under challenging conditions such as low temperatures and water submersion. By studying the effect of water molecules on such CE systems, the authors demonstrated that water acts as a trigger of supramolecular polymerization for controlled adhesive performance.[22c] In contrast, only few cases of the noncovalent cross-linking of CE-based polymers, mainly used as bio-adhesives, have been reported so far. For instance, Liu *et al*. developed a host-guest molecular interactive approach for fabricating molecular engineered CE-protein to achieve a new type of low temperature-tolerated supramolecular adhesives.[1b] Zhao *et al.* utilized CE rings as slidable wheels on the macromolecular chains to obtain mechanically interlocked structures for enhancing mechanical properties.[23] Hence, CE-based architectures show significant potential in developing functional adhesives for various application scenarios in arduous operating environments. Moreover, aside from CE-based adhesives, other supramolecular adhesives designed as hot molten glues or other types of glues require critical curing conditions, such as high temperature[24] and UV light.[5b]

This precludes their use in most applications, which require adhesives operatable at room-temperature and easy to use without additional costs and security concerns. Till now, it remains a great challenge to possess a high adhesive strength of such materials while maintaining other desired capabilities, particularly room-temperature feasibility and mechanical robustness.

Herein, a new type of CE-based supramolecular complex adhesives is developed which is formed at ambient temperature without requiring external trigger, and concomitantly exhibits excellent mechanical strength, versatility on diverse surfaces, and extreme-low temperature tolerance. Four types of tetra-CE terminated polyethylene glycol (TCE-PEG) were designed by chemically linking the CEs to the tetra-arm PEG. By the first time, the CE-based polymer adhesive complex was prepared by supramolecular coordination between tetra-4-aminobenzo-15-crown ether-terminated polyethylene glycol (TCE-PEG-C1) and polyethyleneimine hydrochloride (PEI-HCl). The resulting compound is a dense, strongly interacting supramolecular cross-linked network (TCE-PEG-C1/PEI) with further improved adhesion force. Such supramolecular network can generate strong bonding with various substrates via abundant noncovalent interactions, such as hydrogen bonding, ionic interactions, π-π stacking, and Van der Waals, as well as the reversible chain entanglement of multi-branched macromolecules. Moreover, the TCE-PEG-C1/PEI adhesive can be used at room temperature without intricate curing processes and retains strong adhesion even at low temperatures.

2. Results and Discussion

2.1. Material design

As shown in Scheme 1a, we designed a series of tetra-CE terminated PEG (TCE-PEG) which are composed of tetra-arm PEG skeletons terminated with CE terminal groups through the hexamethylene diisocyanate (HDI) linker. The tetra-arm PEG structure not only provides excellent mechanical properties from the entanglement among polymer chains and multiple supramolecular interactions, but also possesses the intrinsic advantages of PEG polymer itself including flexibility, chemical stability, and moisture sensitivity.

To investigate the effect of CE structures (i.e. ring sizes, reacting groups, and aromaticity) on the adhesive performances, four types of CEs, namely, 4-aminobenzo-15-crown ether, 2-hydroxymethyl-15-crown ether, 4'-aminobenzo-18-crown ether, and 2-hydroxymethyl-18-crown ether (respectively defined as C1, C2, C3, and C4), were selected as the terminal functional groups in this study (synthesis routes shown in Figure S1). The resulting CE-based supramolecular adhesives are denoted as tetra-4-aminobenzo-15-crown ether terminated polyethylene glycol (TCE-PEG-C1), tetra-2-hydroxymethyl-15-crown ether terminated polyethylene glycol (TCE-PEG-C2), tetra-4'-aminobenzo-18-crown ether terminated polyethylene glycol (TCE-PEG-C3), and tetra-2-hydroxymethyl-18-crown ether terminated polyethylene glycol (TCE-PEG-C4, photograph of the four TCE-PEG adhesives shown in Figure S2), respectively. To further investigate the assumption that physical cross-linking will enhance the adhesive performance of supramolecular system, the linear PEI-HCl richly endowed with

secondary amines is chosen as the physical crosslinker complex with the TCE-PEG chains to obtain the supramolecular complex adhesive (TCE-PEG-C1/PEI).

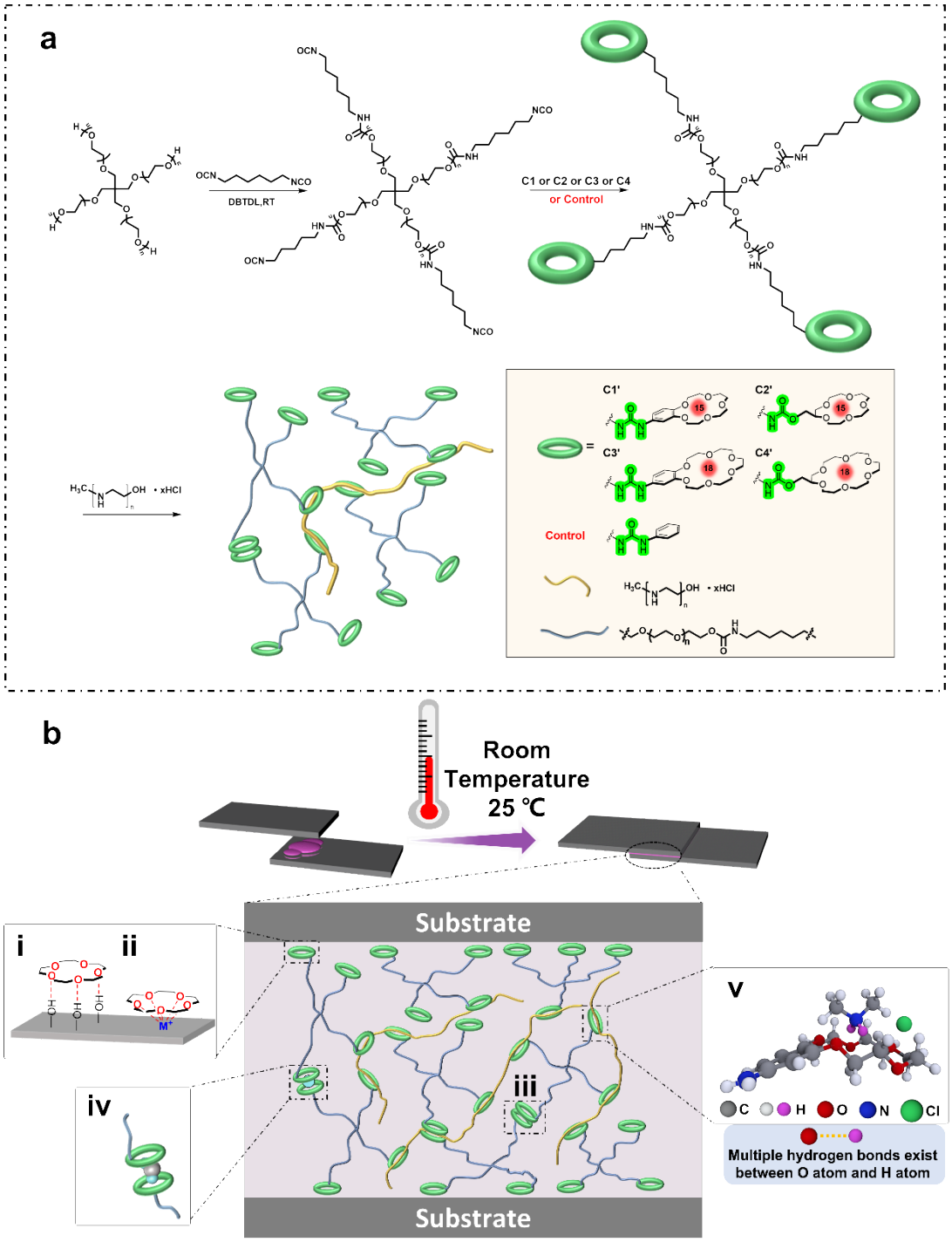

Scheme 1. Schematic illustration of the fabrication of CE-based supramolecular adhesives. a) Synthesis route and chemical structures of four TCE-PEG samples and TCE-PEG-C1/PEI. b) Preparation of the samples for lap-shear test and multiple supramolecular interactions of the TCE-PEG/PEI, including: i) hydrogen bonds between CE rings and hydroxyl groups, ii) coordination interactions from CE rings and

metal ions, iii) Van der Waals force between CE rings, iv) hydrogen bonds between CE rings and water molecules, and v) multiple hydrogen bonds between CE rings and secondary amines.

In view of the multi-physical cross-linking and entangling chains of the TCE-PEG supramolecular network, plenty of physical interactions between the substrate surface and the adhesive, as well as interactions among the multi-arm molecule chains, synergistically contribute to the adhesive performance of the adhesives (Scheme 1b i-v). Adhesion is generally identified as the interfacial binding strength between the adhesives and substrates, while cohesion is defined as the internal strength of the adhesives. These physical interactions play a vital role in improving mechanical performance from both adhesion and cohesion perspectives. (1) On account of the special $–CH_2–O–CH_2–$ ring structure of the CE ring, the O atoms as ideal hydrogen bond acceptors in the CE ring, can form hydrogen bonds with the H atom donors of the substrate surface to improve adhesion (Scheme 1b i).[25] (2) The electrostatic interactions between the positively charged metal ions from the metal substrates and negatively charged O atoms from the CEs also promote the adhesive performance (Scheme 1b ii).[26] (3) Van der Waals forces are generated among CE rings of different chains to enhance cohesion of the system (Scheme 1b iii).[27] The low Gibbs' free energy (ΔG=–11.24 kcal/mol, more details on quantum chemical calculations will be provided later) value for the interactions between two same modified TCE-PEG-C1 molecules also proves the high interaction force due to the above-mentioned supramolecular interactions.

Aside from the above-mentioned interaction among TCE-PEG themselves, some extra molecules also provide additional supramolecular interactions. (4) Some studies[22b, 22c, 28] also reported that CE groups can attract water molecules which would function as the special "bridge" to connect CE rings from different chains, improving cohesion of the system (Scheme 1b iv). (5) The cavities of CEs function as the binding sites for the ammonium groups from PEI-HCl, generating multiple hydrogen bonds as shown in Scheme 1b v. Numerous hydrogen atoms from the secondary amines of the PEI-HCl are capable of bonding to the host CEs to form multiple NH···O hydrogen bonds. Known for the multiple supramolecular physical interactions, the unique supramolecular chemistry enables the TCE-PEG adhesives with excellent cohesion and adhesion performance.

There are several common types of commercially available adhesives including hot molten, two-component mixing, water/solvent evaporation, UV curing, and instant curing (e.g. water vapor trigger) as listed in Table S1. The TCE-PEG adhesives are operatable at room-temperature and easy to use without pretreatment like pre-mixing and heat/light triggers, making the TCE-PEG design competitive for widely using.

2.2. Structural Characterization

To validate the synthesized products, ^{1}H NMR, FTIR, and GPC measurements were conducted with respect to the chemical structure, composition, and molecular weight. The terminated hydroxyl groups of tetra-arm-PEG were modified to isocyanate groups by HDI, and the product is confirmed by the disappearance of proton signals corresponding to the hydroxyl groups of tetra-PEG-OH at 2.81 ppm (Figures S3-S4).

At the same time, the characteristic peak of $–CH_2$ adjacent to the isocyanate groups at 3.29 ppm and the peak of $–CH_2$ adjacent to the urethane groups at 3.15 ppm are observed with integral areal ratio being 1:1, confirming the successful formation of tetra-PEG-NCO without significant cross-linking. After further terminal reaction to form TCE-PEG, for example TCE-PEG-C1, the characteristic peaks ascribed to the $–CH_2–O–CH_2–$ of CE rings are observed at the range of 3.7-4.2 ppm (peaks e, f, and g in Figure 1a), and the proton signals adjacent to the isocyanate groups disappear (peak d in Figures 1b). The similar variation can also be observed in all the synthesized TCE-PEG (Figures S5-S8). As illustrated by the FT-IR spectra of TCE-PEG-C1 in Figure 1c, the disappearance of characteristic peak of isocyanate group at 2249 cm^{-1} can further verify the successful grafting reaction of isocyanate groups on the hydroxyl (or amine) units, as well as other TCE-PEG cases in Figure S9. In addition, the gel permeation chromatography (GPC) result reveals a slight shift of molecular weight (from 1900 g/mol of tetra-PEG-OH to 2600 g/mol of tetra-PEG-NCO, Figure 1d) after the terminal modification, consistent with the theoretical molecular weights and the ^1H NMR results.

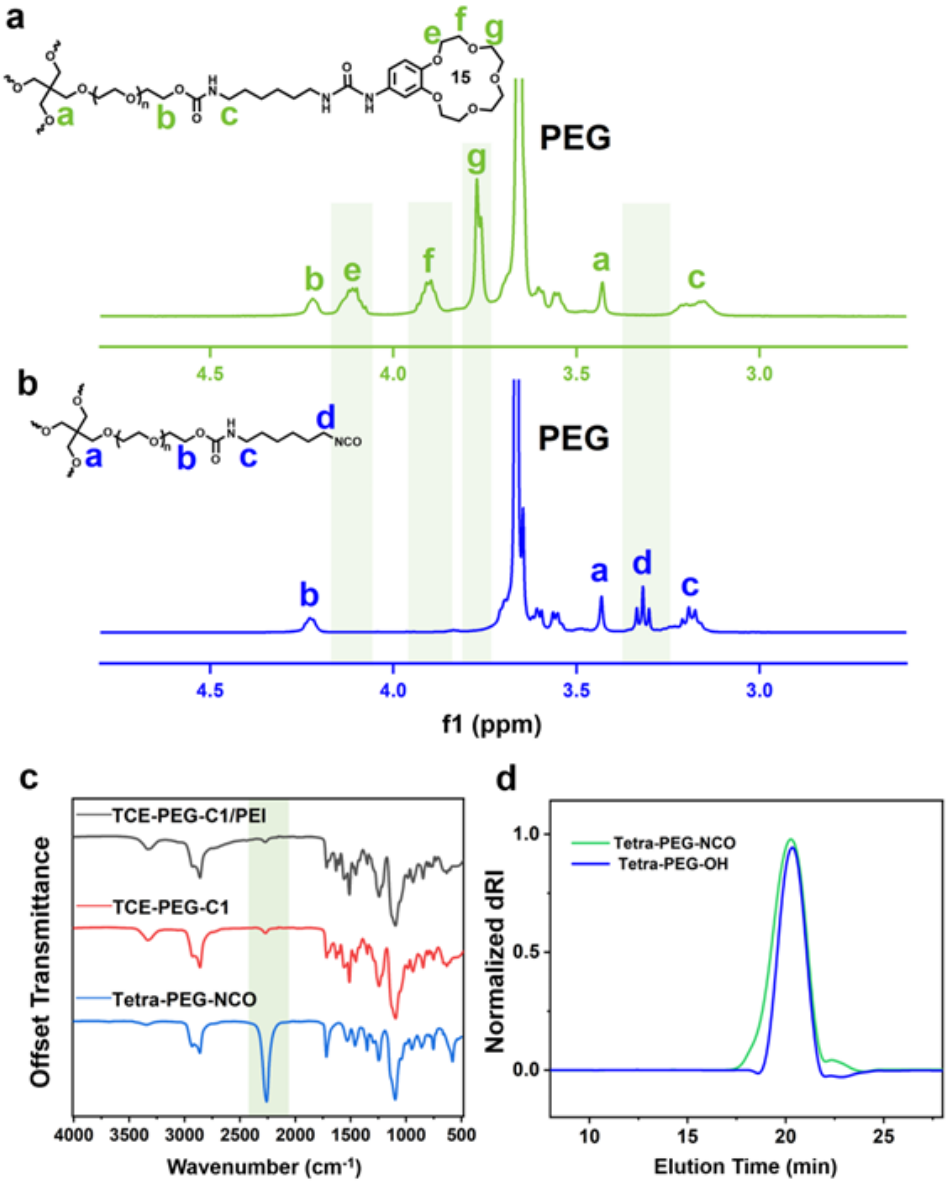

Figure 1. a) The ^{1}H NMR spectrum of TCE-PEG-C1. b) The ^{1}H NMR spectrum of tetra-PEG-NCO. c) FT-IR spectra of the tetra-PEG-NCO, TCE-PEG-C1, and TCE-PEG-C1/PEI. d) GPC spectra of the tetra-PEG-NCO and tetra-PEG-OH.

Thermogravimetric analysis (TGA) was carried out to investigate the thermal behaviors of the TCE-PEG-C1, TCE-PEG-C2, TCE-PEG-C3, and TCE-PEG-C4, and their decomposition temperatures are all higher than 200 °C (Figure 2a). The TCE-PEG-C1 shows the highest decomposition temperature among the samples, indicating its decent thermostability and strong noncovalent interactions. As illustrated by

differential scanning calorimetry (DSC) curves in Figure 2b, the glass transition temperatures (T_gs) of the TCE-PEG-C1, TCE-PEG-C2, TCE-PEG-C3, and TCE-PEG-C4 are in the range of –43 °C to –35 °C. The T_gs of TCE-PEG-C1 and TCE-PEG-C3 are slightly higher than those of the TCE-PEG-C2 and TCE-PEG-C4. This discrepancy can be attributed to the presence of π-π stacking interactions between the benzene rings and the intermolecular interactions among the polar groups in TCE-PEG-C1 and TCE-PEG-C3. This result further confirms the significance of intermolecular interactions in influencing the thermodynamic behavior of the polymers.

To further investigate the microstructure in the adhesive complex, the SAXS of tetra-PEG-OH, TB-PEG, TCE-PEG-C1, and TCE-PEG-C1/PEI were characterized as shown in Figure 2c and Figure S10. Similar to that of the tetra-PEG-OH, scattering peaks centered at 1.53 $Å^{-1}$ can be observed in the SAXS curves of TB-PEG, TCE-PEG-C1, and TCE-PEG-C1/PEI. Such long-range ordered structure is proposed as the characteristic distance between tetra-arm-PEG aggregates,[29] which is impervious to the presence of noncovalent interactions (e.g. benzene ring, CE, complexation) at room temperature. Furthermore, it can be also observed that both TB-PEG and TCE-PEG-C1/PEI display a broad peak around 0.70 $Å^{-1}$, and the q value of the peak in TB-PEG (0.89 $Å^{-1}$) is larger than that in TCE-PEG-C1/PEI (0.64 $Å^{-1}$), suggesting the larger domains with distinct electron density in TCE-PEG-C1/PEI. Considering the π-π stacking interactions involving benzene rings existed in TB-PEG, as well as the coordinating effects of CE rings and secondary amine structure existed in TCE-PEG-C1/PEI, it is speculated that the degree of micro-phase separation is greater in the TCE-

PEG-C1/PEI system. This is attributed to the size difference between the two structures, and the size of the region involving interactions between CE rings and secondary amines is larger than that of the benzene ring. Unlike the aforementioned, the SAXS curve of the TCE-PEG-C1 sample does not exhibit such characteristic peak in the region. The size of the interaction units between crown ether rings are relatively large, making it unobservable at the Ångström scale. Additionally, the steric hindrance between the crown ether rings prevents the appearance of benzene stacking, as observed in TB-PEG.

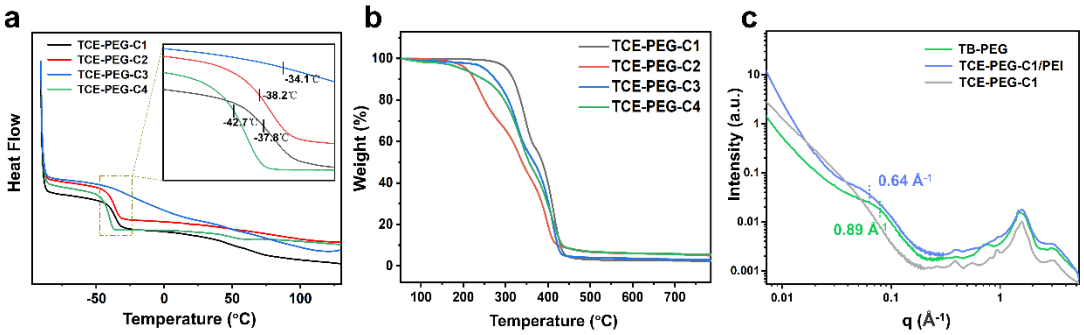

Figure 2. a) DSC curves of the four TCE-PEG adhesives. b) Thermogravimetric analysis (TGA) data of the four TCE-PEG adhesives. c) SAXS curves of the TB-PEG, TCE-PEG-C1, and TCE-PEG-C1/PEI.

2.3. Adhesive Performance of CE-based adhesives

With CE as terminal units, the TCE-PEG adhesives show excellent adhesion on various surfaces, visually demonstrated by a few simple adhesion tests as shown in Figure 3a. The lap-shear tests were conducted to evaluate the adhesion strength of synthesized adhesives with different substrates including paper, paperboard, glass, wood, aluminum, and steel. The TCE-PEG adhesives were applied between two slides of the designated substrate with an overlapping area of 144 mm^2 under a pressure ~ 340 kPa at room temperature. The reliable physical network with multiple interactions and chain

entanglement was built after sufficient time without additional heating process. Figure 3b illustrates the effect of CE structure on the lap-shear strength of the TCE-PEG-C1, TCE-PEG-C2, TCE-PEG-C3, and TCE-PEG-C4 adhesives. The TCE-PEG-C1 shows the highest adhesive strength under ambient conditions (25 °C and 50 RH%), and the values are 4.21, 3.10, and 3.00 MPa on the wood, steel, and aluminum substrates, respectively. The typical stress-strain curve of the TCE-PEG-C1 adhesive being applied on wood substrates is shown in the inset of Figure 3b, which suggests a low strain upon substrate separation (~ 10%). This could be attributed to the strong multiple interactions between molecules, as well as the relatively low molecular weight of the chains between physical cross-links. Due to the ultra-high adhesive performance, some substrates (glass, paper, and paperboard) broke themselves before the bonding layer fractured, as shown in Figure S11. The adhesive strength discrepancy of the TCE-PEG-C1 being applied on different substrates mainly depends on the chemical groups on the surfaces, in which hydrogen bonding is primarily formed for wood, glass, and paper while metal complexation is primarily formed for metal. It could be speculated that the effect of hydrogen bonding plays a more significant role than that of the metal on adhesive performance for the TCE-PEG adhesives.

Compared with the TCE-PEG-C1, the TCE-PEG-C3 displays a slightly weaker adhesion on these surfaces. As shown in Figure 3b and Table S1, the adhesion strength of the TCE-PEG-C3@Wood (3.50 MPa, the TCE-PEG-C3 adhesive bonded wooden sheets, the same below), TCE-PEG-C3@Steel (0.40 MPa), and TCE-PEG-C3@Aluminum (0.20 MPa) are 17%, 87% and 93% compared with those of the TCE-

PEG-C1 counterparts, respectively. Such discrepancy is even larger for the cases of TCE-PEG-C2 and TCE-PEG-C4, which can be ascribed to the weaker interactions from their CE structures and the formed urethane units. In comparison, there are aromatic and urea groups in the TCE-PEG-C1 and TCE-PEG-C3, suggesting stronger physical interactions from π-π stacking and hydrogen bonding among their urea groups. Especially, a loading experiment for the TCE-PEG-C1 bonding two wood substrates using 24 kg weight was conducted to showcase its excellent adhesive performance (Figure 3c, using 40 kg weight in Movie S1). To further showcase the adhesive in usage scenario, a plastic hook sticking on a door using TCE-PEG-C1 is presented in Figure S12, and up to 10 kg weight can be loaded for a long period of time.

The adhesive properties of the TCE-PEG adhesives curing for seven days (at room temperature in air) are compared in Figure S13 for the stability demonstration. All TCE-PEG adhesives cured after seven days almost show improved adhesive performance on different substrates compared to those curing for one day. Among the four types of adhesives, such enhancement is most significant for TCE-PEG-C1. The increment in adhesion strength of the TCE-PEG-C1@Wood (5.50 MPa), and TCE-PEG-C1@Steel (4.23 MPa) TCE-PEG-C1@Aluminum (3.71 MPa) curing for seven days are 30%, 36%, and 24%, respectively, compared with the counterparts (Figure S14). This indicates that the TCE-PEG adhesives would progressively achieve superior adhesive performance over time through further curing, which can be explained that the direct exposure of samples to air allows water molecules to form hydrogen bonds with the CE rings. FTIR measurement of the TCE-PEG-C1 with different water contents was conducted to

demonstrate the effect of water molecular on the chemical structure of resulting adhesive (Figure S15). An increased intensity can be obviously observed at a band of 3548 cm^{-1}, which is attributed to the hydrogen bonding (structured) state formed with the existence of water molecules.[22b] As such, water molecules behave as cross-linkers to connect multiple CE molecules together to finally improve the cohesion of the system.[1b] With stable adhesion of TCE-PEG-C1 at room temperature, the underwater adhesion of TCE-PEG-C1 on wood substrates stored in water for 1h was subsequently investigated as shown in Figure S16. The underwater adhesive strength of TCE-PEG-C1 can still retain almost 60% (4.23 MPa) of its original adhesive strength, which is significantly higher than those in the recently reported CE-based systems.[1b, 22a] In general, the excess free water absorbed in the adhesive increases the molecular chain spacing and weakens the intermolecular interactions. The high retention of adhesive performance at underwater condition could be ascribed to the multiple strong molecular interactions, which demonstrated excellent water resistance and the potential for underwater application.

To investigate the role of CE moiety on adhesion properties, tetra-benzene terminated polyethylene glycol (TB-PEG) was also prepared as a control by replacing the CE with benzene rings. As shown in Figure 3d, the adhesion strength of TB-PEG @Paperboard and TB-PEG@Glass are 0.89 and 0.64 MPa, respectively. The decrement in adhesion strength of the TB-PEG@Aluminum (0.51 MPa) and TB-PEG@Wood (0.78 MPa) are 81% and 83%, respectively, as compared with those of the TCE-PEG@Aluminum and TCE-PEG@Wood. This is explained that the absence of CE

rings results in weaker intermolecular interactions and adhesion, comprehensively proving the significant role of CE rings for the structure design. Overall, several control studies were performed to demonstrate the contribution of various supramolecular interactions on enhancing adhesive strength (details in Supporting Information). The hydrogen bonding would be dominant for adhesion enhancement, and water molecular cross-links would be responsible for cohesion enhancement.

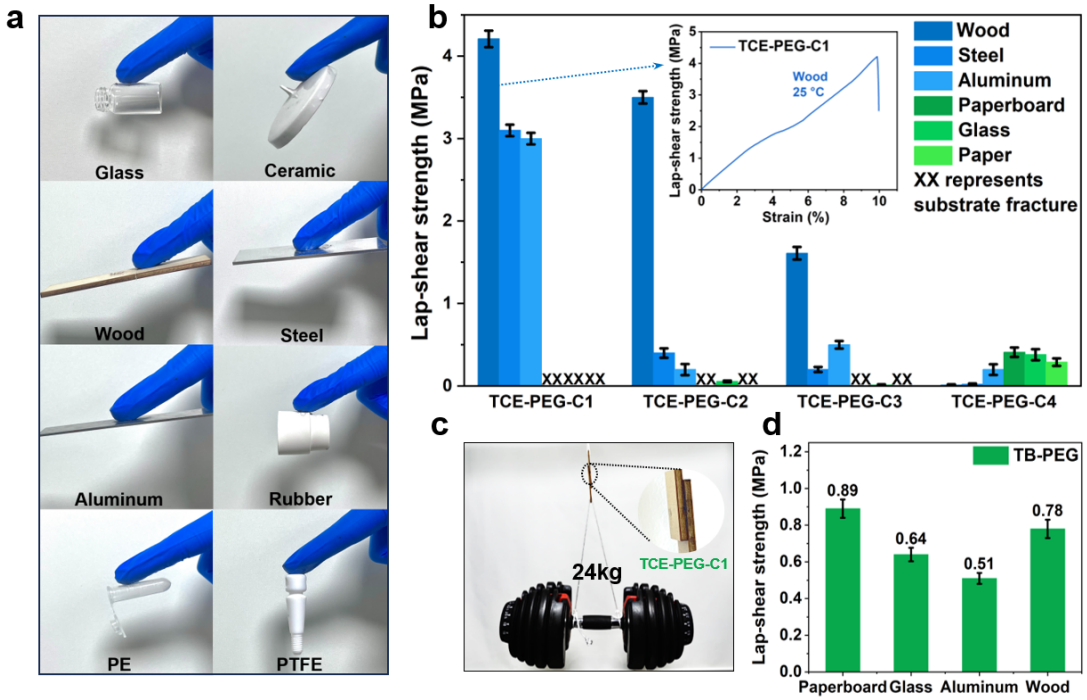

Figure 3. a) Photographs showing the adhesiveness of the TCE-PEG-C1 adhesives with various substrates including glass, ceramics, steel, rubber, PE and PTFE. b) Lap-shear strength of TCE-PEG-C1, TCE-PEG-C2, TCE-PEG-C3, and TCE-PEG-C4 on different substrates at 25 °C and 50 RH%. The inset shows the stress-strain curve of the TCE-PEG-C1 adhesive on wood. c) The loading experiment for the TCE-PEG-C1 bonding two wood substrates using 24 kg weight, and the overlapping area is 120 mm^2. d) Lap-shear strength of the control sample TB-PEG on different substrates.

It is significant for adhesive to be used under extreme environments like low-temperature conditions. To investigate the low-temperature applicability, quantitative lap shear tests of TCE-PEG-C1 adhesives on diverse substrates were firstly tested at −15 °C. As shown in Figures 4a and 4b, although a slight decline in adhesion

performance is observed, the adhesion strength of TCE-PEG-C1@Wood and TCE-PEG-C1@Steel can still maintain at 2.0 MPa and 1.5 MPa, respectively. Especially, less than 10% loss in the adhesion strength of the TCE-PEG-C1@Aluminum is observed. Based on the quantitative test, the adhesion behavior showcase of the TCE-PEG-C1 adhesive in liquid nitrogen was further investigated. The adhesive strength of the TCE-PEG-C1 on various substrates were further measured under different low temperatures in Figure S17. As the curing temperature decreased, the adhesive strength of TCE-PEG-C1 reduced with different substrates. This can be explained that the segment relaxation of molecular chains becomes slower at low temperature, which allows a weaker stretchability and hence easy cracking of the system. In spite of this, the adhesive property is still tolerable under low temperature (1 MPa to 2 MPa), which could be attributed to the presence of bound water as confirmed by FTIR. The formation of water clusters can be significantly impeded at low temperatures, averting stress concentrations and cracking.[1b] As shown in Figure 4c, the TCE-PEG-C1 adhesive still exhibits decent adhesion even at –196 °C. It can also maintain adhesive even after experiencing rapid temperature changes (i.e., upon returning to room temperature). These observations illustrate that the TCE-PEG-C1 achieves not only excellent adhesion performance at low-temperature environments but also exceptional resistance to significant temperature fluctuations.

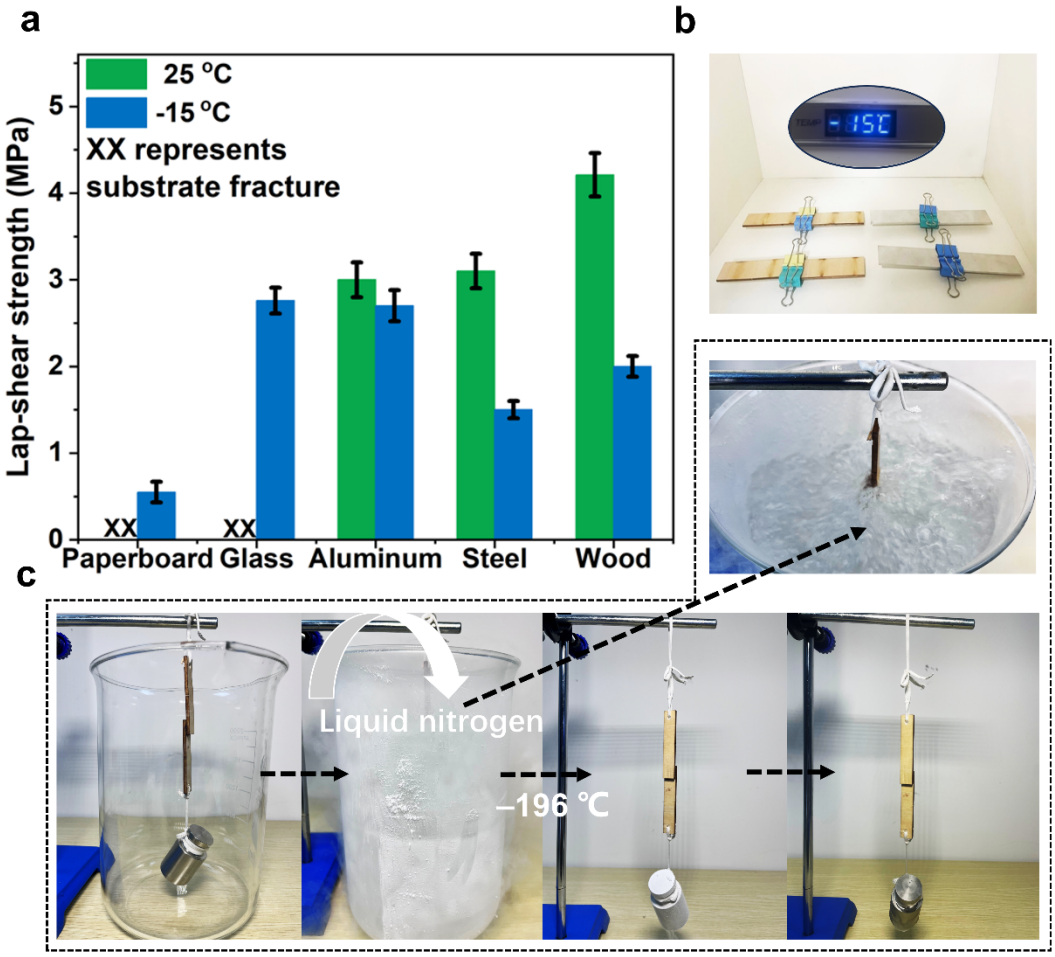

Figure 4. a) Comparison of lap-shear strength of the TCE-PEG-C1 adhesive between the low-temperature environment (–15 °C) and room temperature. b) The photograph of the samples stored at –15 °C for lap-shear test. c) Macroscopic adhesion tests of TCE-PEG-C1 bonding two wood substrates (144 mm^2) in liquid nitrogen.

2.4. CE-based supramolecular adhesives *via* PEI complexation

To further investigate the complexation effect of CEs for improved adhesion performance of CE-based adhesive, the optimized sample, i.e. TCE-PEG-C1, as the matrix is selected to mix with the linear polymer PEI-HCl. The adhesion strength of TCE-PEG-C1/PEI on different substrates (wood, aluminum, and steel as shown in Figure 5a) are 7.21 MPa, 3.88 MPa, and 4.82 MPa, respectively, exhibiting a significant improvement compared to the pristine sample TCE-PEG-C1. Particularly for the case

using wood substrates, the increment in adhesion strength of the TCE-PEG-C1/PEI@wood (7.21 MPa) were 31% of that of the TCE-PEG-C1 (5.50 MPa). The significantly improved adhesive properties are attributed to the coordination interaction between the secondary amines in the PEI and the cyclic CE structure. Macrocycles with an CE cavity are suitable hosts for complexing protonated ammonium ions, thus achieving stable coordination by accepting hydrogen bonds with the nucleophilic heteroatoms of the host, namely, through NH···O hydrogen-bonding interactions between the ammonium groups of cations and the O atoms of CEs.[30] Moreover, the incorporation of linear polymers remarkably enhances the entanglement of molecular chains within the network structure, rendering the enhanced cohesion. Those two molecular level interactions synergistically stabilize the supramolecular polymeric adhesive system and yield excellent lap-shear strength.

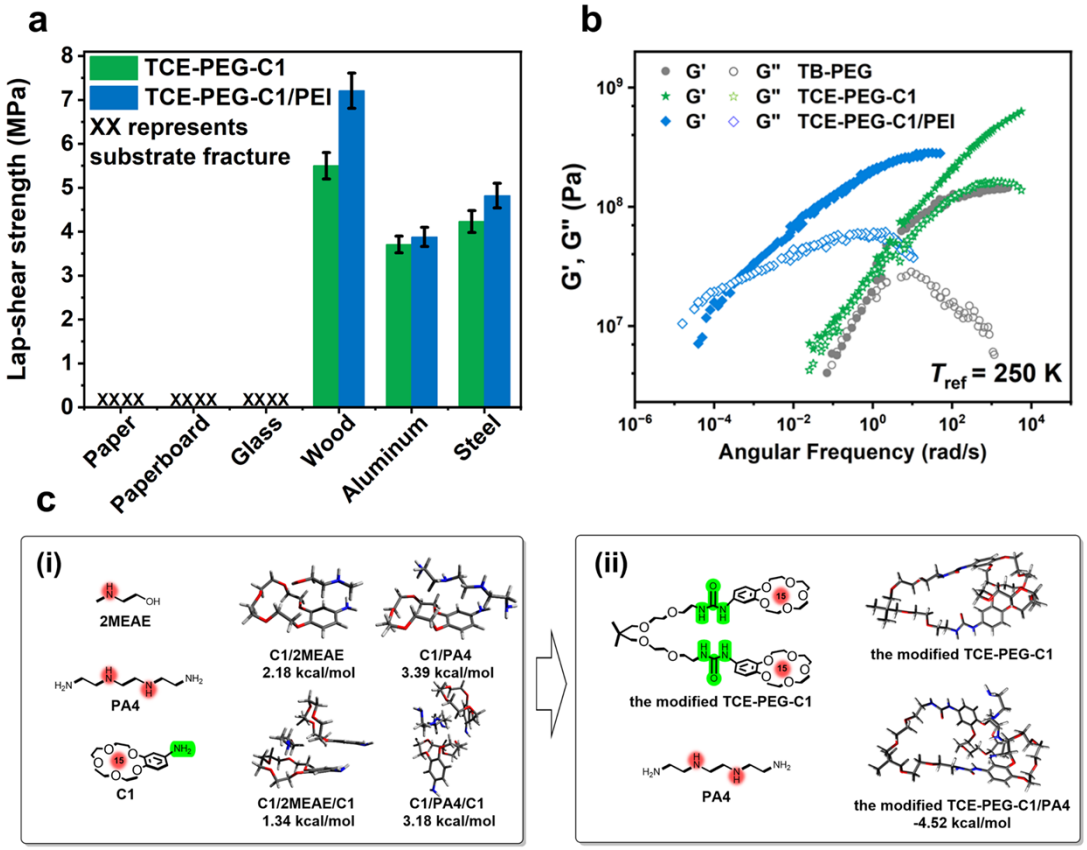

Figure 5. a) Comparison of lap-shear strength between the TCE-PEG-C1 and TCE-PEG-C1/PEI adhesives. b) Oscillatory shear responses of TB-PEG (gray circles), TCE-PEG-C1 (green stars), and TCE-PEG-C1/PEI (blue diamonds) presented in terms of frequency-dependent G′ (solid symbols) and G″ (open symbols) master curves. c) DFT simulations on the complexing interaction between the CE rings and secondary amine. i) Small molecule system: 2MEAE, PA4, and C1; ii) Tethered system: the modified TCE-PEG-C1 and PA4.

The shear adhesion strength of the complexing adhesives, TCE-PEG-C1/PEI, with different mixing ratios was also tested on wood substrates. It is observed that with increased amount of PEI-HCl, the adhesion strength of TCE-PEG-C1/PEI exhibits an initial rise followed by a subsequent decrease as shown in Figure S18. This phenomenon can be explained from the view of the relationship between adhesion and cohesion. The increment is ascribed to the cohesion improvement in the TCE-PEG-C1 by the physical interaction between secondary amines and CE rings. However, as the number of CE rings coordinating with secondary amines increases, the number of CE

rings interacting with the substrate surface decreases, resulting in a decrement in adhesion. The TCE-PEG-C1/PEI mixture blended at a ratio of 1:0.05 achieves an ultra-high lap-shear strength of 7.21 MPa. However, with such ratio optimized under room temperature, the complexation effect and entanglement of molecular chains were suppressed at low temperatures, rendering lower adhesion strength (Figure S19).

To highlight the advantages of the current design of CE-based adhesive, the adhesive properties of the recently reported CE-based adhesives are listed in Table S3. It shows that the adhesive strength of TCE-PEG-C1/PEI is superior to most of the reported results except for the one using biomacromolecules. Our TCE-PEG-based adhesive system also presents mild curing condition and unique availability in low temperature and underwater conditions. However, a limitation for CE-based adhesives in commercial application is the cost of the CEs (e.g. ~ 344 USD/g for C1 in our case) is higher compared with other adhesive systems using commodity polymers. As awareness of the advantages of CE-based adhesive raises, the cost may decrease if industry develops new advanced fabrication methods.

Shear rheology is also firstly performed on the resulting supramolecular complex adhesives to support the explanation above. For covering broad dynamic ranges, the individual spectra probed at different temperatures were collapsed with respect to the data recorded at a given temperature to form master curves, following well-known rheological procedures.[31] The viscoelastic responses of TCE-PEG-C1 and TCE-PEG-C1/PEI are presented in Figure 5b where we also included, for reference purposes, the corresponding results obtained for a control sample of TB-PEG. To allow a direct

comparison, the master curves for all three materials have been constructed using the same reference temperature of 250 K. The control sample (TB-PEG, gray symbols) displays a shear response which is typical for an oligomeric system, with the structural relaxation (reflecting the segmental dynamics) as the dominant relaxation feature. The spectral fingerprint of the latter is a pronounced peak in the $G''(\omega)$ curve, which features a characteristic frequency of about 10 rad/s for the selected reference temperature. Its corresponding instantaneous shear modulus G_∞, defined as the high-frequency limit of the storage modulus G', is relatively low, i.e., ~ 0.1 GPa. The TCE-PEG-C1 adhesive (green symbols) exhibits a more complex shear response with a noticeable contrast between the segmental dynamics and the low-frequency terminal relaxation, and the latter is similar with the one displayed by the control material. We note that the corresponding G_∞ for TCE-PEG-C1 approaches 1 GPa, implying a higher rigidity of this system at low temperatures with respect to the control one. Finally, the shear response of the TCE-PEG-C1/PEI mixture (blue symbols) shows a clear separation between the segmental (1 rad/s) and terminal (10^{-1} rad/s) relaxation rates, and the presence of strong intermediate spectral contribution resembled the situation of strongly cross-linked polymers network. Since the terminal relaxations directly relates to the macroscopic flow in these materials, the results in Figure 5b additionally reveal that at a given temperature the steady-state viscosity of TCE-PEG-C1/PEI is significantly larger than that similarly featured by TCE-PEG-C1 and TB-PEG.

To further reveal the mechanism of the interaction between TCE-PEG-C1 and PEI-HCl, the quantum chemical calculations on simple and complex systems that can

elucidate the influence of complexing interactions on the supramolecular network at the molecular level were also performed. A series of molecules were used for the simulation as summarized in Figures 5c and S20, and various supramolecular orientations were generated and optimized using DFT followed by frequency calculations to determine of the change in Gibbs' free energy (ΔG). For the simple system (Figure 5c i), two linear small molecules, i.e., 2-(methylamino)ethanol (2MEAE) and triethylenetetramine (PA4), were chosen as guests for the adhesion enhancement of TCE-PEG-C1/PEI, and the C1 was selected as the host. Due to the considerable repulsive interaction for C1/2MEAE, the guest molecule is unlikely to penetrate through the center of the CE, consistent with the previous study.[20b] As illustrated by the stabilized molecular geometries of C1/2MEAE and C1/PA4 complex systems in Figure 5c i, the computed Δ*G* for C1/MAEA=1:1 and C1/PA4=1:1 systems are 2.18 kcal/mol and 3.39 kcal/mol, respectively. The ΔG for C1/MAEA=1:2 and C1/PA4=1:2 systems are comparable (1.34 and 3.18 kcal/mol, respectively) and lower than those with the ratio of 1:2. The results suggest that more amine groups result in less stable systems with weaker intermolecular interactions and lower ΔG for the C1 crown ether variant. The opposite was observed for C2 and C3, where more amine groups resulted in more stable systems.

Furthermore, tethered systems were designed, due to the inconsistent behaviors using the untethered crown ether systems, for the interaction between the modified TCE-PEG-C1 and PA4 to elucidate the adhesive performance. Figure 5c ii shows an example of the optimized structure of the modified TCE-PEG-C1 and the TCE-PEG-C1/PA4

interacting system. To simplify the computation, there are only two arms extending from the central C atom of the modified TCE-PEG-C1 with the other two arms replaced by methyl groups. The ΔG of interacting system between the modified TCE-PEG-C1 and PA4 shows the lowest values among the cases with different CE rings (–4.52 kcal/mol, Figure 5c ii), confirming the stable supramolecular complexation between TCE-PEG-C1 and PEI-HCl.

3. Conclusion

A series of novel TCE-PEG-based ultra-strong adhesives with multiple physical interactions are designed using tetra-armed PEG terminated with CE rings and linear polymer PEI-HCl as noncovalent crosslinks for further improved adhesion performance. The TCE-PEG adhesives can be directly processed at ambient temperature, and no extra conditions (e.g. heating or UV) are required for the curing process. Importantly, the TCE-PEG-based adhesives also exhibit durable adhesive behavior, excellent underwater stability, and low temperature tolerance. Incorporation of linear polymer PEI-HCl in the TCE-PEG system not only provides a higher density of physical crosslinks but also enhances the noncovalent interactions through the multiple hydrogen bonding between secondary amines and CE rings, achieving a strong supramolecular adhesive network with a lap-shear strength of 7.21 MPa. Such innovative design has been experimentally demonstrated to be effective in adhesive performance and enriches the supramolecular adhesive family, and the adhesive performance surpasses most of the reported CE-based adhesives. The efficient

complexation between TCE-PEG-C1 and PEI-HCl is further confirmed by the calculated ΔG along with the comparative rheological master curves and steady-state viscosities of TCE-PEG-C1, TB-PEG, and TCE-PEG-C1/PEI. It is anticipated that the developed supramolecular adhesive system with multiple noncovalent interactions will be a unique strategy for the advanced fabrication of high-performance adhesives in various challenging environments.

Supporting Information

Supporting Information is available from the Wiley Online Library or from the author.

Acknowledgements

This work was supported by the National Natural Science Foundation of China (grant no. 52373275 and 52303290) and Vehicle Technologies Office in the Department of Energy (grant no. VTO CPS 36928). Part of this work was carried out at the Center for Nanophase Materials Sciences, Department of Energy, Office of Science user facility.

Conflict of Interest

The authors declare no conflict of interest.

Data Availability Statement

The data that support the findings of this study are available from the corresponding author upon reasonable request.

Reference:

[1] a) C. R. Westerman, B. C. McGill, J. J. Wilker, *Nature* **2023**, 621, 306; b) K. Zhao, Y. Liu, Y. Ren, B. Li, J. Li, F. Wang, C. Ma, F. Ye, J. Sun, H. Zhang, K. Liu, *Angew. Chem. Int. Ed.* **2022**, 61, e202207425; c) M. Liu, Z. Wang, P. Liu, Z. Wang, H. Yao, X. Yao, *Sci. Adv.* **2019**, 5, eaaw5643; d) X. Liu, Q. Zhang, L. Duan, G. Gao, *ACS Appl. Mater. Interfaces* **2019**, 11, 6644; e) M. A. Gebbie, W. Wei, A. M. Schrader, T. R. Cristiani, H. A. Dobbs, M. Idso, B. F. Chmelka, J. H. Waite, J. N. Israelachvili, *Nat. Chem.* **2017**, 9, 473; f) Y. Gao, J. Zhao, Z. Huang, T. K. Ronson, F. Zhao, Y. Wang, B. Li, C. Feng, Y. Yu, Y. Cheng, D. Yang, X. J. Yang, B. Wu, *Angew. Chem. Int. Ed.* **2022**, 61, e202201793; g) Y. Liu, J. Wan, X. Zhao, J. Zhao, Y. Guo, R. Bai, Z. Zhang, W. Yu, H. W. Gibson, X. Yan, *Angew. Chem. Int. Ed.* **2023**, 62, e202302370.

[2] a) A. Faghihnejad, K. E. Feldman, J. Yu, M. V. Tirrell, J. N. Israelachvili, C. J. Hawker, E. J. Kramer, H. Zeng, *Adv. Funct. Mater.* **2014**, 24, 2322; b) S. Chen, K. Zhang, Z. Li, Y. Wu, B. Zhu, J. Zhu, *Supramol. Mater.* **2023**, 2, 100032.

[3] L. Xie, L. Gong, J. Zhang, L. Han, L. Xiang, J. Chen, J. Liu, B. Yan, H. Zeng, *J. Mater. Chem. A* **2019**, 7, 21944.

[4] a) K. Kim, M. Shin, M.-Y. Koh, J. H. Ryu, M. S. Lee, S. Hong, H. Lee, *Adv. Funct. Mater.* **2015**, 25, 2402; b) Y. Xu, Y. Ji, J. Ma, *Langmuir* **2020**, 37, 311.

[5] a) N. Holten-Andersen, A. Jaishankar, M. J. Harrington, D. E. Fullenkamp, G. DiMarco, L. He, G. H. McKinley, P. B. Messersmith, K. Y. C. Lee, *J. Mater. Chem. B* **2014**, 2, 2467; b) C. Heinzmann, S. Coulibaly, A. Roulin, G. L. Fiore, C. Weder, *ACS Appl. Mater. Interfaces* **2014**, 6, 4713.

[6] a) S. Baik, H. J. Lee, D. W. Kim, J. W. Kim, Y. Lee, C. Pang, *Adv. Mater.* **2019**, 31, 1803309; b) Y. Ma, S. Ma, Y. Wu, X. Pei, S. N. Gorb, Z. Wang, W. Liu, F. Zhou, *Adv. Mater.* **2018**, 30, 1801595.

[7] Y. Ahn, Y. Jang, N. Selvapalam, G. Yun, K. Kim, *Angew. Chem. Int. Ed.* **2013**, 52, 3140.

[8] J. Wu, H. Lei, X. Fang, B. Wang, G. Yang, R. K. O'Reilly, Z. Wang, Z. Hua, G. Liu, *Macromolecules* **2022**, 55, 2003.

[9] a) W. Xu, Y. Nan, Y. Jin, X. Chen, M. Xie, C. Chen, C. Zhao, *Chem. Mater.* **2022**, 34, 8740; b) K. V. Dikshit, A. M. Visal, F. Janssen, A. Larsen, C. J. Bruns, *ACS Appl. Mater. Interfaces* **2023**, 15, 17256.

[10] a) J. Li, Y. Zhang, Q. Zhang, C. Cai, F. Li, S. Dong, *Adv. Mater. Interfaces* **2022**, 10, 2202005; b) J. Zhu, S. Zhao, J. Luo, W. Niu, J. T. Damron, Z. Zhang, M. A. Rahman, M. A. Arnould, T. Saito, R. Advincula, A. P. Sokolov, B. G. Sumpter, P.-F. Cao, *CCS Chem.* **2023**, 5, 1841.

[11] Y. Zhao, Y. Wu, L. Wang, M. Zhang, X. Chen, M. Liu, J. Fan, J. Liu, F. Zhou, Z. Wang, *Nat. Commun.* **2017**, 8, 2218.

[12] X. Li, Z. Wang, W. Li, J. Sun, *ACS Mater. Lett.* **2021**, 3, 875.

[13] a) J. Cui, D. Daniel, A. Grinthal, K. Lin, J. Aizenberg, *Nat. Mater.* **2015**, 14,

790; b) B. Li, S. Ge, S. Zhao, K. Xing, A. P. Sokolov, P.-F. Cao, T. Saito, *Mater. Horiz.* **2023**, 10, 2868.

[14] a) R. Du, J. Wu, L. Chen, H. Huang, X. Zhang, J. Zhang, *Small* **2014**, 10, 1387; b) J. Li, S. Luo, F. Li, S. Dong, *ACS Appl. Mater. Interfaces* **2022**, 14, 27476.

[15] C. Cai, H. Gong, S. Wu, F. Li, S. Liu, Z. Tan, S. Dong, *Chem. Eng. J.* **2023**, 451, 138674.

[16] X. Liu, J. Xu, X. Xie, Z. Ma, T. Zheng, L. Wu, B. Li, W. Li, *Chem. Commun.* **2020**, 56, 11034.

[17] Y. Hong, F. Zhou, Y. Hua, X. Zhang, C. Ni, D. Pan, Y. Zhang, D. Jiang, L. Yang, Q. Lin, Y. Zou, D. Yu, D. E. Arnot, X. Zou, L. Zhu, S. Zhang, H. Ouyang, *Nat. Commun.* **2019**, 10, 2060.

[18] G. M. Whitesides, *Angew. Chem. Int. Ed.* **2018**, 57, 4258.

[19] J. Zhou, P. Han, M. Liu, H. Zhou, Y. Zhang, J. Jiang, P. Liu, Y. Wei, Y. Song, X. Yao, *Angew. Chem. Int. Ed.* **2017**, 56, 10462.

[20] a) C. J. Pedersen, *Science* **1988**, 241, 536; b) C. J. Pedersen, *J. Am. Chem. Soc.* **1967**, 89, 7017.

[21] a) F. Nicoli, M. Baroncini, S. Silvi, J. Groppi, A. Credi, *Org. Chem. Front.* **2021**, 8, 5531; b) J. Zhang, H. Qiu, T. He, Y. Li, S. Yin, *Front. Chem.* **2020**, 8, 560.

[22] a) X. Li, Y. Deng, J. Lai, G. Zhao, S. Dong, *J. Am. Chem. Soc.* **2020**, 142, 5371; b) Q. Zhang, T. Li, A. Duan, S. Dong, W. Zhao, P. J. Stang, *J. Am. Chem. Soc.* **2019**, 141, 8058; c) S. Dong, J. Leng, Y. Feng, M. Liu, C. J. Stackhouse, A. Schönhals, L. Chiappisi, L. Gao, W. Chen, J. Shang, L. Jin, Z. Qi, C. A. Schalley, *Sci. Adv.* **2017**, 3, eaao0900; d) T. Li, Q. Zhang, D. Li, S. Dong, W. Zhao, P. J. Stang, *ACS Appl. Mater. Interfaces* **2020**, 12, 38700; e) X. Li, J. Lai, Y. Deng, J. Song, G. Zhao, S. Dong, *J. Am. Chem. Soc.* **2020**, 142, 21522.

[23] a) J. Zhao, Z. Zhang, C. Wang, X. Yan, *CCS Chem.* **2024**, 6, 41; b) J. Zhao, Z. Zhang, L. Cheng, R. Bai, D. Zhao, Y. Wang, W. Yu, X. Yan, *J. Am. Chem. Soc.* **2022**, 144, 872.

[24] P. Sun, Y. Li, B. Qin, J.-F. Xu, X. Zhang, *ACS Mater. Lett.* **2021**, 3, 1003.

[25] a) H. S. Biswal, S. Wategaonkar, *J. Phys. Chem. A* **2010**, 114, 5947; b) M. Solimannejad, S. Scheiner, *Chem. Phys. Lett.* **2006**, 429, 38.

[26] a) G. Olsen, J. Ulstrup, Q. Chi, *ACS Appl. Mater. Interfaces* **2015**, 8, 37; b) X. Wang, J. Hu, T. Liu, G. Zhang, S. Liu, *J. Mater. Chem.* **2012**, 22, 8622; c) J. D. Rodriguez, J. M. Lisy, *J. Am. Chem. Soc.* **2011**, 133, 11136.

[27] H.-J. Schneider, *Angew. Chem. Int. Ed.* **2009**, 48, 3924.

[28] X. Li, B. Lv, X. P. Zhang, X. Jin, K. Guo, D. Zhou, H. Bian, W. Zhang, U. P. Apfel, R. Cao, *Angew. Chem. Int. Ed.* **2022**, 61, e202114310.

[29] J. Luo, X. Zhao, H. Ju, X. Chen, S. Zhao, Z. Demchuk, B. Li, V. Bocharova, J. Y. Carrillo, J. K. Keum, S. Xu, A. P. Sokolov, J. Chen, P. F. Cao, *Angew. Chem. Int. Ed.* **2023**, 62, e202310989.

[30] a) P. Vezse, B. Benda, A. Fekete, A. Golcs, T. Toth, P. Huszthy, *Molecules* **2022**, 27, 2838; b) M. Kubo, M. Kida, S. Muramatsu, Y. Inokuchi, *J. Phys. Chem. A* **2020**, 124, 3228; c) D. Zhou, H. Hao, Y. Ma, H. Zhong, Y. Dai, K. Cai, S. Mukherjee, J. Liu, H. Bian, *J. Phys. Chem. B* **2020**, 124, 9154; d) R. M.

Izatt, J. D. Lamb, N. E. Izatt, B. E. Rossiter, Jr., J. J. Christensen, B. L. Haymore, *J. Am. Chem. Soc.* **1979**, 101, 6273.

[31] S. P. Bierwirth, C. Gainaru, R. Böhmer, *J. Chem. Phys.* **2018**, 148, 221102.